Uniform-intensity, visible light source for *in situ* imaging

Eyal Bar-Kochba
Saagar Govil
Stony Brook University
Department of Materials Science and Engineering
Stony Brook, New York 11794-2275

Jon P. Longtin
Stony Brook University
Department of Mechanical Engineering
Stony Brook, New York 11794-2300

Andrew Gouldstone
Northeastern University
Department of Mechanical and Industrial Engineering
Boston, Massachusetts 02115-5000

Mary D. Frame
Stony Brook University
Department of Biomedical Engineering
Stony Brook, New York 11794-8181

Abstract. A flexible, low-cost, high-brightness light source for biological and biomedical imaging is presented. The illuminating device consists of a custom-size square plastic pouch 10 to 20 mm on a side and 1 to 3 mm thick that can be inserted fully or partially into both *in situ* or *in vitro* specimens to be imaged. The pouch contains a silicone-based gel medium embedded with silica particles that scatters light and provides a reasonably uniform, planar light source. Light is delivered to the pouch using a multimode optical fiber and a high-intensity tungsten lamp. Pouch size and geometry can be readily altered as needed for a particular application. Benefits of the device include reasonably uniform light intensity, low temperature rise (<2 °C), a nearly white light spectrum, and a thin (<2 mm thick) flexible form factor. The design, fabrication, and preliminary results from the device are presented using hamster cheek pouch tissue, with comparisons to standard intravital microscopy, along with suggestions for further improvement and potential uses. [DOI: 10.1117/1.3103334]

Keywords: light source; transillumination; *in situ* microvascular observations; *in vivo* microscopy; fiber optic; low temperature; white light.

Paper 08328R received Sep. 12, 2008; revised manuscript received Jan. 25, 2009; accepted for publication Jan. 28, 2009; published online Apr. 28, 2009.

1 Introduction

Optical diagnostics and microscopy are ubiquitous in biology, physiology, and biomedical engineering. Examples include optical spectroscopy of tissue,[1,2] *in vivo* tumor detection,[3] cellular tissue analysis,[4] and emerging imaging techniques.[5–7] In many applications, the final quality of the optical image depends strongly on the illuminating light source. This is particularly true for transmission-based studies in which tissue is placed between the light source and imaging system, e.g., during traditional bright-field microscopy. For such applications, a light source with a spatially homogeneous intensity distribution is desired.

Furthermore, although histological specimens are often used, a number of studies exist in which one would like to image the tissue less invasively in order to observe function *in situ*, e.g., blood vessel diameter or flow. Consider for example the specific case of the *gracilis* muscle. This particular tissue is well suited for investigation of integrative biological states, such as neurogenic inflammation, which is linked to clinical conditions ranging from sports injury pain to migraine headaches.[8,9] However it must be studied *in situ*, so that the origin and insertion of the muscle to the bone is not disrupted and so that there is minimal to no damage to the vascular and nerve supply. Simply using epi-illumination (light directed toward the muscle surface) is inadequate for imaging the affected blood vessels and blood flow.

The ideal light source would be nondestructive in that it would be mechanically deformable, would generate minimal heat, and would be thin enough to place underneath muscle layers, while still providing homogeneous and intense illumination. To the authors' knowledge, no such device currently exists.

In this study, we have designed and fabricated a flexible, low-heat light source with homogeneous intensity using a fiber optic inserted into a flexible pouch containing a scattering medium. The scattering medium is a colloidal suspension of silicate particles inside a polydimethylsiloxane (PDMS) silicone elastomer. Silica has well-known scattering properties, high visible light transmission ($>95\%$), and a refractive index of 1.45 to 1.47 for white light. PDMS was used because it is optically clear, inert, and flexible. Pouch preparation and silicate concentration were varied to determine the optimal optical and thermal characteristics. In addition, the resulting device was tested *in vivo* with experiments on hamster cheek pouch tissue for comparison to standard bright-field microscopy.

The presented device could be readily extended to the ultraviolet and infrared spectral regions with appropriate choice of components. Also a short-pulse laser source could be used for illumination as well in place of the continuous-wave (CW) tungsten lamp, thus providing many of the benefits of short pulse laser techniques. Importantly, this thin light pouch can be used to provide transillumination in a less invasive manner than current fiber-optic methods, thus preserving the tissue to a greater extent.

2 Design Goals

Several factors drove the preliminary design presented in this work. These include:

Address all correspondence to: Jon P. Longtin, Stony Brook University, Department of Mechanical Engineering, Stony Brook, NY 11794-2300. Tel: 631-632-1110; Fax: 631-632-8544; E-mail: jlongtin@ms.cc.sunysb.edu

1083-3668/2009/14(2)/024024/7/$25.00 © 2009 SPIE

• **Minimal thickness**—Since the light source is designed to be placed underneath a variety of tissues, thinness is a primary factor. In this work, a target thickness of 2 to 3 mm was set.

• **Flexibility**—As the light source will be inserted into and positioned underneath tissues, the ability for the device to bend to conform to the tissue contour is desired.

• **Uniform light intensity**—The light source is desired to be as uniform as possible, particularly since it will be used to identify small or low-contrast structures within the specimen.

• **Large area**—A target illumination area of up to 20 $\times$ 20 mm was used in this study.

• **High brightness**—Many biological tissues are both strongly scattering and strongly absorbing; hence, a high photon flux is desired to maximize contrast and resolving capability.

• **Low temperature**—As the light source is being used *in vivo* or *in vitro*, a temperature rise of less than 5 °C within the device due to either optical or electrical heating was desired.

• **True white light**—Ideally, the light source will cover a range of wavelengths, as is typical for white light. Monochromatic light sources are less desirable, because they limit the detection of potential features, particularly those similar in color to the incident light.

The preceding requirements precluded several conventional light source technologies. For example, traditional filament-based light sources generate temperatures far too high to be inserted directly into an organism and are too large for this application. Light emitting diodes (LEDs) do not generate significant heat and can be made small; however, their light is nearly monochromatic, and it is also challenging to arrange a collection of LEDs into a uniform light source. Electroluminescent light sources have low luminosity and require high operating voltages (50 to 100 V).

Fiber optics are used extensively as light sources; however, they do have several disadvantages for the types of imaging tasks discussed ealier. Light emerging from single fibers diverges dramatically as one moves away from the fiber end, with the light field behaving more like a point source rather than a plane source. Fiber bundles come closer to producing a planar light source; however, the discrete nature of each fiber will result in significant intensity variation as the magnification approaches the distance between the fibers. For example, if the fiber strands in the bundle are 100 μm in diameter, then the resulting light distribution would be very uneven for microscopy of objects 200 to 300 μm in size (the typical microscopy field used for microvascular observations).

For these reasons, a fiber-optic-based light source that utilizes a scattering medium for the illuminating device placed within the animal was chosen for this work. This choice was found to be the best compromise, given the preceding design criteria, and provides additional benefits such as ease of manufacture, low cost, the avoidance of electrical voltages to be placed within the body, and sterilizability.

3 Experimental Setup

Figure 1 shows the experimental setup used in this work. A 150-DLC continuous-wave (CW) tungsten lamp illumination source (Ram Optical Instrumentation, Inc., Rochester, New York) is used as the light source. Light intensity can be varied by changing the voltage to the bulb. The light output is coupled to a flexible multifilament fiber bundle 1.2 m long with a core diameter of 6.35 mm that can be positioned as needed for light delivery. The fiber bundle also serves as a high-pass optical filter: over 90% of the radiation generated from the tungsten lamp is in the infrared region, which results in heating but no visible light output.[10] The optical transmission region of the fiber bundle is such that nearly all of the infrared radiation generated by the lamp is absorbed by the fiber, thus allowing only visible light to exit the opposite end of the fiber. This dramatically reduces the heating associated with infrared radiation passing into the illumination pouch.

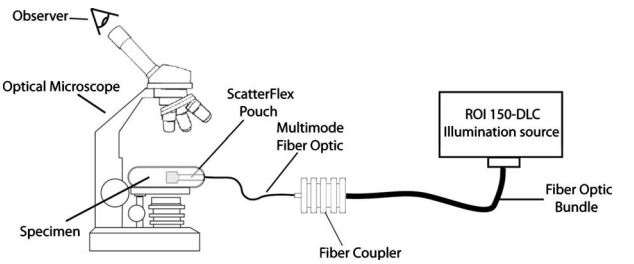

Fig. 1 Schematic of experimental layout, including light source, fiber bundle, fiber coupler, multimode fiber optic, and illumination pouch.

A second fiber optic cable is used to transfer the light from the tungsten lamp to the pouch. This fiber optic is a silica-core multimode fiber (ThorLabs, Inc., Newton, New Jersey) The fiber is 1 m long with a core diameter of 1.0 mm, a 2.5-mm protective sheathing, and a numerical aperture of 0.48. One end is bare terminated, and the other is terminated with a sub miniature version A (SMA) connector by the manufacturer. The SMA end is coupled to the end of the light source fiber bundle using a free-space arrangement in which the fiber bundle and fiber optic are spaced 1 mm apart and centered along their optical axes. Both cables are secured in a custom-made aluminum coupler that provides mechanical stability as well as heat dissipation for any residual infrared radiation that may pass through the light source bundle. This simple, optics-free coupling arrangement results in a lower coupling efficiency than if focusing elements were used; however, sufficient light is still coupled into the multimode fiber for illumination purposes, due primarily to the high brightness of the light source. Future designs would benefit from a more efficient light coupling or a redesign of the entire light source itself, thus reducing the illumination requirements of the source.

The opposite end of the fiber is inserted into the pouch after being cleaved using a fiber cutting tool. The freshly cleaved end of the fiber is left unpolished, which provides additional scattering at the fiber end, as polishing removes the rough edges and irregularities from the fiber end face. The bare end of the fiber emits light into a flexible pouch containing a highly scattering medium, which is the portion of the system that is inserted into the specimen for illumination. Approximately 12 mm of the fiber sheathing was removed before inserting the end of the fiber into the pouch.

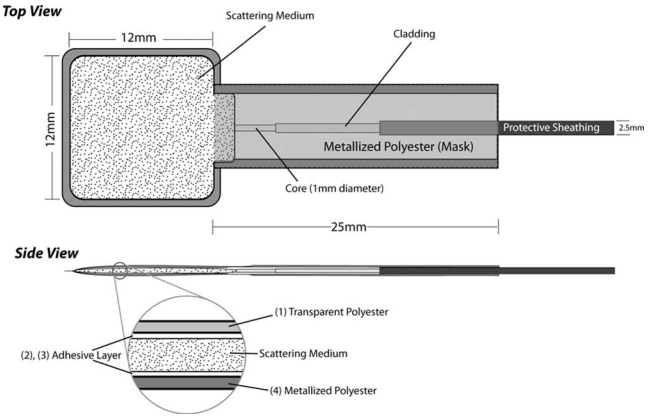

Fig. 2 Pouch detail. (Top) View of pouch from above. Fiber-optic light supply enters pouch from the left. (Bottom) Side view of pouch showing multilayer structure and scattering media.

3.1 *Pouch Design*

The heart of the system is a flexible polymer pouch filled with a mixture of a silicon-based elastomer and small silica particles (Fig. 2). The pouch consists of four distinct polymer layers (UltraFlex Packaging Corp, Brooklyn, New York) [Fig. 2(a)]. The top layer (1) is made of optically transparent polyester, while the bottom layer (4) is made of a metallized polyester, which reflects light back into the medium. Layers 2 and 3 are adhesive layers of linear low-density polyethylene (LLDPE) that were used to create a seal between layers 1 and 4 when heated. The scattering medium is located between layers 2 and 3. The bare end of the fiber is inserted into the medium in the pouch, where light emanates from the bare end of the fiber cable, is then scattered throughout the pouch medium, and eventually exits through the top transparent layers of the pouch.

The pouch is fabricated by layering the polymer sheets in their appropriate order over a rubber mat, after which the edges are sealed using a hot stamp heated to a temperature of 275 to 300 °C and moderate hand pressure for 5 s. A thin sheet of Teflon between the stamp and the polymer layer prevents adhesion to the stamp. Two pouch sizes were fabricated; the first pouch was 20×20 mm by 3 mm thick and was used for the optical characterization. A second smaller pouch 10×10 mm by 2 mm thick was fabricated and used for the animal studies.

3.2 *Scattering Medium*

The scattering medium is a silicate powder of mostly silica composition prepared via the solvent evaporation method using an acid solution [ethanol, hydrochloric acid, and (high-performance liquid chromatography HPLC)—grade water] with tetraethylorthosilicate (TEOS) as the silica source. The solution was heated on a hot plate on medium heat to evaporate all liquid, leaving a solid layer of silicate; this process took roughly 1 h. The silicate was removed and crushed using a mortar and pestle for 10 min to produce a fine powder. The silicate particle morphology was imaged by sputter-coating powder samples with ~12 nm of gold in an Edwards S150b coating unit (Wilmington, Massachusetts) and placing in an LEO 1550 scanning electron microscope (SEM; Thornwood, New York) operating at 20 kV with a Robinson backscatter detector and a working distance of 9 mm.

The scattering medium was mixed into the PDMS silicone elastomer (Sylgard 184, Dow Corning, Midland, Michigan) precure (10:1 base:curing mass% mixing ratio) with concentrations of 20, 30, 40, 50, and 60 mass% silicate particles. The pouch was filled with the liquid mixture immediately after mixing using a syringe, after which it was placed in a vacuum desiccator for 4 h at 65 °C to remove air bubbles and cure the elastomer. Last, the bare end of the optical fiber was inserted into the pouch and secured with double-sided tape wrapped around the fiber.

3.3 *Specimen Preparation and Microscopy*

The hamster cheek pouch tissue was chosen to evaluate this light source for two reasons. First, it is similar in thickness to the hamster *gracilis* muscle (400 to 800 μm), which is a tissue for which this light pouch is particularly well suited. The total transmittance of light through the cheek pouch is similar to that through the *gracilis*. Second, the cheek pouch tissue is readily exteriorized without compromising the vasculature. Thus, a comparison of the *same* vascular location is possible using standard bright-field transmitted light and the fabricated light pouch.

All animal studies were performed with the approval of the Animal Care and Use Committee for Stony Brook University. Adult male hamsters (124 ± 12 grams, $N=4$) were anesthetized (pentobarbital sodium, 70 mg/kg) and tracheostomized, and the right cheek pouch was prepared for intravital microscopy.[11] Briefly, the tissue was gently everted from the lateral side of the mouth and pinned over a quartz pillar; typically, the bright-field light passes through the quartz pillar and tissue for observation. The cheek pouch tissue was observed using a modified Nikon upright microscopy with a 25 $\times$ objective (Leica, NA=0.65), using both a collimated bright-field light source (halogen lamp) with a long working distance condenser and the light pouch device. The light pouch (10 mm $\times$ 10 mm $\times$ 2 mm) was slid under the cheek pouch tissue between the tissue and the quartz pillar. Images were captured using an intensified charge coupled device (ICCD) camera (Solamere Technology Group, Inc.) and videotaped with an SVHS Panasonic AG 7350 recorder. Analog images were digitized offline (EPIX, XCap, Inc.), and blood vessel diameters were measured using ImageJ (freeware, NIH). Comparisons of diameters for the same vascular location with the different light sources were made using a paired *t*-test with $\alpha=0.05$.

4 Results and Discussion

4.1 *Scanning Electron Microscope Analysis of Silicate Morphology*

Scanning electron microscope (SEM) images of the silicate powder at different magnifications are shown in Fig. 3. The powder consists of small granular particles of varying size. The actual size distribution depends on the crushing operation. For this particular sample, the larger particles have a mean edge length of about 150 μm, with a standard deviation of 24 μm, as estimated from Adobe Photoshop. For the

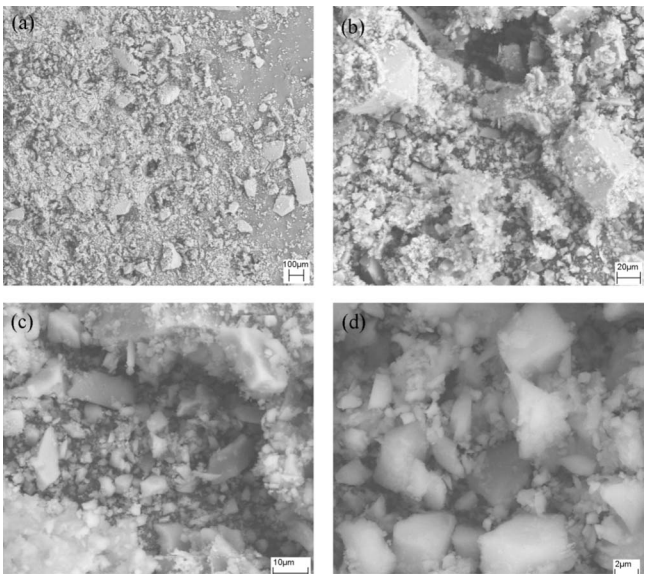

Fig. 3 SEM images of the silicate particles that were used to scatter the incoming light in the pouch. Magnifications of (a) 125×, (b) 1,000 ×, (c) 3,000×, and (d) 30,000×.

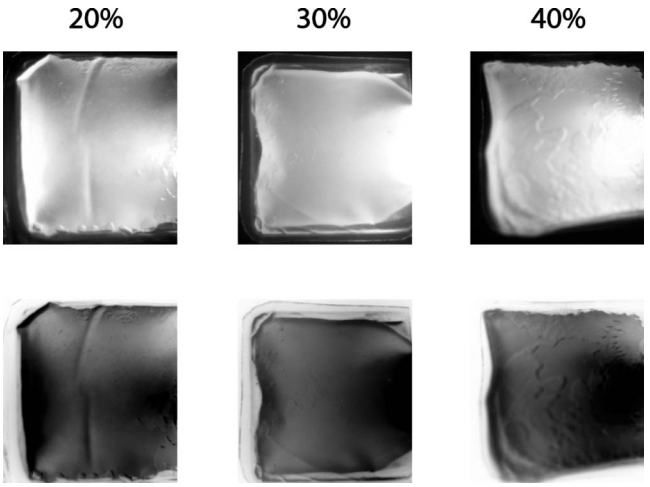

Fig. 4 (Top) Grayscale photographs of light intensity from the pouch for concentrations of 20% (left), 30% (middle), and 40% (right) silica by weight. (Bottom) Same images shown in inverse to highlight regions of small intensity variation. Inverse images can also be used as filters to make the light distribution more uniform (see text).

higher magnification figures [Figs. 3(c) and 3(d)], it can be seen that the larger particles have a highly angular morphology that corresponds to rhombohedral cleavage, characteristic of quartz. The smaller particles are also angular; however, they are more equi-axed than the larger particles [Figs. 3(c) and 3(d)]. The mean edge length for the smaller particles was 6.5 μm, with a standard deviation of 0.99 μm.

4.2 *Characterizing Illumination Uniformity*

Silicate particle morphology, size, and concentration play a strong role in the light scattering process. As some of the particles are on the order of microns in size, Mie scattering theory holds,[12] but it is complicated by the nonspherical nature of the silicate particles.[13] In this work, the optimal (most uniform) light distribution was determined empirically by fabricating devices with different silica concentrations, supplying light, and visually determining the optimal concentration.

Figure 4 shows a top view of the illuminated pouch for particle concentrations of 20%, 30%, and 40%. The fiber enters the pouch from the left side. For the 20% silicate concentration (Fig. 4, left), much of the light emitted from the fiber end strikes the pouch edges, where it is either reflected, transmitted, or absorbed, as seen on the left of the top row in the figure for the 20% concentration. The highest silica concentration of 40% (Fig. 4, right), on the other hand, results in a high luminosity near the fiber end with a rapid decrease in intensity away from the end, due to strong scattering by the media. A reasonably uniform brightness was achieved with a silicate weight percentage of 30%, as shown in the center of Fig. 4. Negatives of the top images, shown in the bottom row of Fig. 4, better illustrate the intensity variation across the pouch. Also, as discussed here, the negative of the intensity distribution can be used as a grayscale filter that can be used to provide a more uniform light source.

Even with the 30% concentration, the region near the end of the delivery fiber exhibits a higher than average brightness. Significant improvements in uniformity can still likely be made, and the detailed analysis and optimization of the device scattering properties are opportunities for future research.

To determine the absolute intensity distribution of the pouch a Tenma 72-6693 light meter was used (Tenma, Centerville, Ohio). The 30% concentration pouch was placed in a dark room, and the light meter was used to record the total brightness, L_{tot} from the pouch (in lux). The pouch was also imaged during this time with a Canon PowerShot SD-600 at an image resolution of 6.0 megapixels. To make the data processing more manageable, the image was down-sampled in Adobe Photoshop to a total of $N=52,275$ pixels and converted to an 8-bit grayscale image with each pixel intensity, p_j, ranging from 0 (darkness) to 255 (saturation). The brightness of each pixel, B_j, is then computed from the pixel intensity as

$$B_j = \beta p_j, \quad \text{where } \beta = \frac{L_{tot}}{\frac{N}{\sum_{j=1} p_j}}. \tag{1}$$

Here, β is a conversion factor from grayscale to lux. The results are shown in Fig. 5. For this image, the constant β was found to be 0.37, resulting in a maximum pixel brightness of 94 lux ($0.37 \cdot 255 \approx 94$). Note the saturated region (light gray semicircular plateau) near the fiber end. The brightness here exceeded the maximum pixel value and thus represents some information loss. It can be seen that the intensity values are high near the fiber end and decrease as one moves away from the fiber end. The distribution is nearly radially symmetric, and there is a modest increase in intensity near the edges, where the incident light strikes the pouch boundaries. It should be noted that the fiber enters the pouch from below in this figure, rather than from the side, as in Fig. 4.

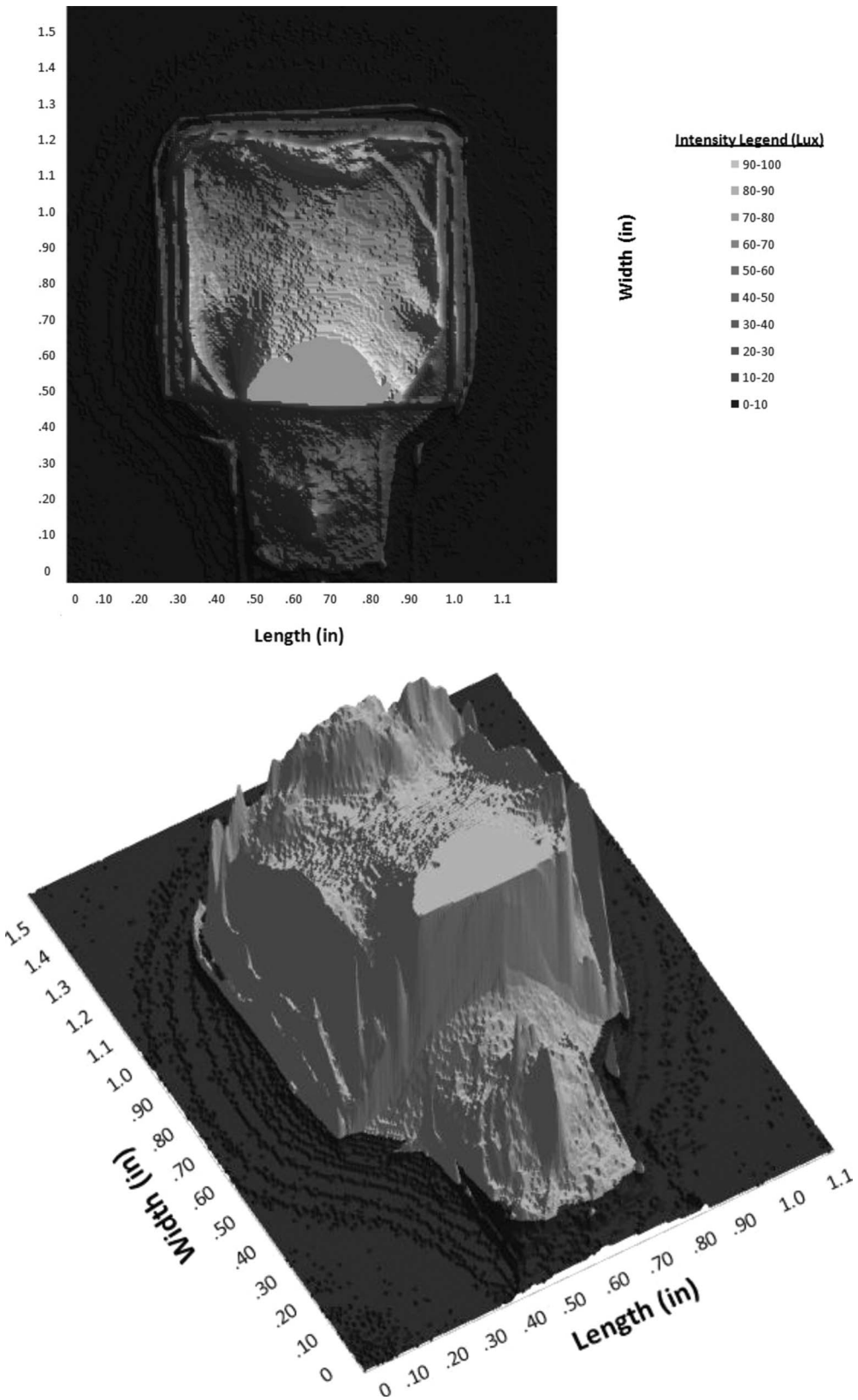

Fig. 5 Absolute intensity distribution in the pouch on a per-pixel basis. (Top) 2-D image. Illuminating fiber enters from bottom. Notic the saturated region near the fiber end. (Bottom) 3-D image of same, showing intensity distribution in the pouch.

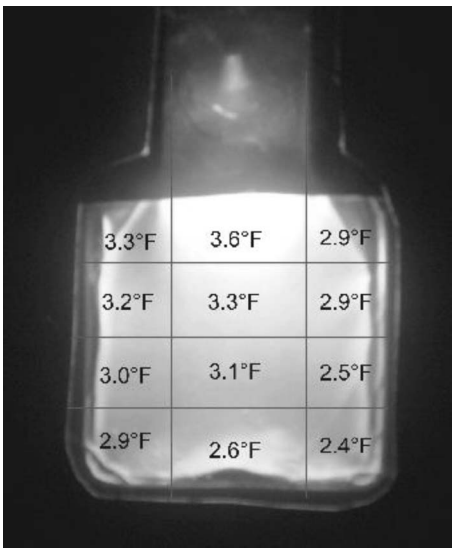

Fig. 6 Measured temperature increase *above* ambient for different regions of the pouch. The thermocouple was placed in contact with the pouch and left in place until the temperature reading stabilized.

4.3 *Temperature Distribution*

A key design factor is to ensure that the pouch does not generate appreciable heat when in use. To assess the temperature rise of the device during operation, the system was turned on for 15 min. A 0.5-mm-diam. K-type thermocouple (Omega Engineering, response time ~10 ms) was then placed in contact with different areas of the top of the pouch, and the temperature was recorded once the reading stabilized. Results are shown in Fig. 6 expressed as the measured temperature increase *above* ambient temperature, which was 27.2 °C (81.1°F) measured using the same thermocouple setup. The temperature rise is highest near the fiber end and decreases away from it. In all cases, the temperature rise is less than 2.2 °C (4.0°F), which meets the 5 °C design requirement stated earlier. Furthermore, in actual use, the pouch will be surrounded by tissue, which has a significantly greater cooling capability than air, and thus the temperature rise in the pouch will be even less than that measured in ambient air.

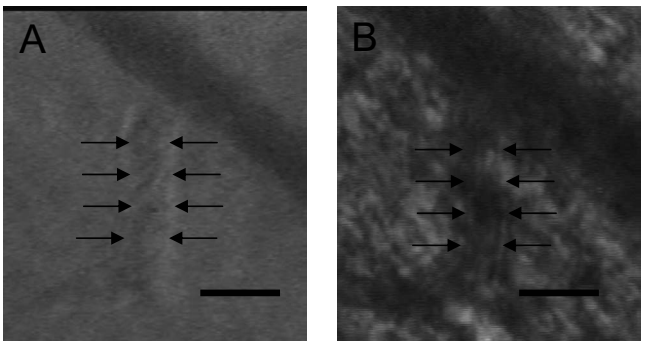

Fig. 7 Video images of the same vascular location in the hamster cheek pouch taken with (a) the pouch device transmitted light and (b) bright-field transmitted light. Arrows denote the walls of the in-focus arteriole. Scale bars are 20 microns.

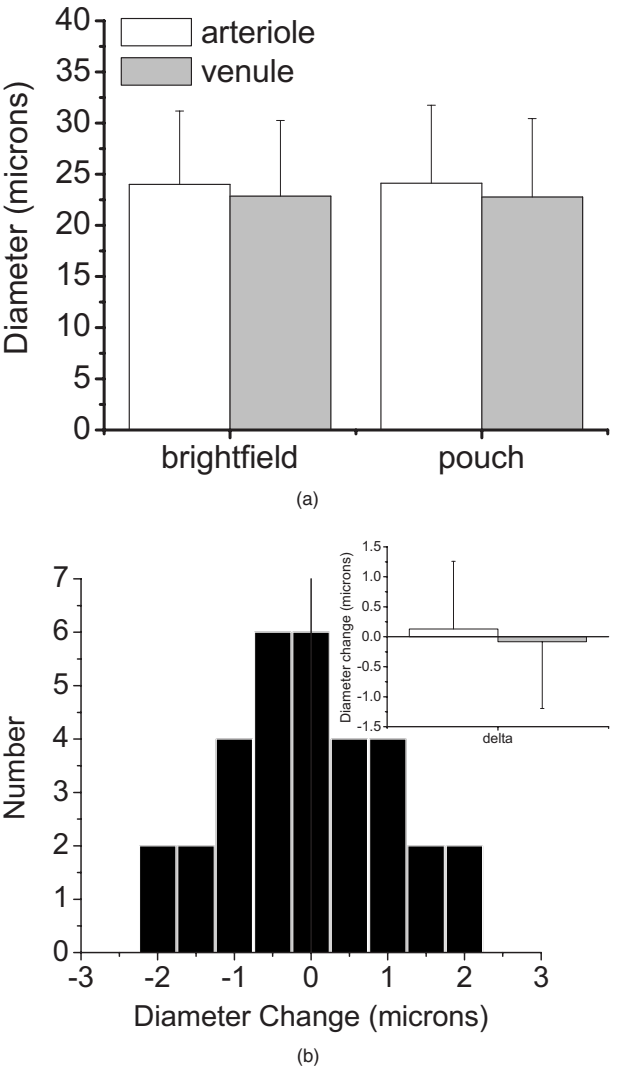

Fig. 8 (a) The mean±stddev of the $n=16$ imaged arteriole and venule diameters using bright-field or the pouch device transmitted light. Four vessels of each type were observed in each of four hamsters. (b) A histogram of the difference between the pouch and bright-field diameter measurements (pouch–bright-field) for all vessels ($n=32$). The inset shows the mean±stddev of the diameter difference ($p=0.90$).

4.4 *In Vivo Optical Microscopy*

Visual comparisons of the same microvascular location (Fig. 7) provide evidence that the transmitted light is collimated with our standard bright-field light source (as expected) and diffuse with the fabricated pouch device (also as expected). Fine detail of the tissue structure is better seen with the collimated light; thus, the pouch light system is not likely to replace standard microscopy for histological work. Unlike histological microscopy, however, we sought a means to evaluate physiological function in a *noninvasive* manner in developing the light source. The main criterion for a suitable light source to determine function in intravital microscopy is the ability to measure distances accurately. To this end, we compared the measured blood vessel diameter using both standard bright-field microscopy and the fabricated pouch device. Two blinded observers measured $N=32$ vessel diameters at the same vascular locations using both bright-field and

pouch-transmitted light sources. The average diameter of arterioles and venules from all measurements is shown in Fig. 8(a) for each light source. The difference in diameter as measured with the two light sources for each measurement location is shown in Figure 8(b). As can be seen, measured values are all within ± 2 μm (about 10%), with over half (18/32) within ± 0.5 μm ($\sim 2\%$). Thus, despite the fact that qualitative images can appear considerably different (Fig. 7), measured functional parameters such as diameter are in very good agreement compared to traditional bright-field microscopy.

5 Conclusions and Further Work

This work presents the preliminary design, fabrication, and testing of a flexible illumination device used for *in vivo* imaging and microscopy. The device uses silicate particles as scattering agents embedded in a flexible silicone-based medium encased in a flexible pouch. Light is provided via a multimode optical fiber and a tungsten lamp. The device provides a minimally invasive, diffuse light source that permits microvascular measurements with minimal tissue dissection. Repeated measures of living systems can thus be obtained, including in clinical settings with human patients. The device was demonstrated by observing and measuring a key functional parameter of microvessel diameter with hamster cheek microcirculation and comparing the measurements made to those using standard bright-field microscopy. The thin (2 to 3 mm) form factor, easily alterable size, and flexible nature of the device are particularly useful for such applications.

There are many opportunities for further refinement of the device. Suggestions include optimizing the scattering media type, concentration, and particle size distribution to obtain as uniform a light distribution as possible. This could be done in conjunction with analytical and numerical tools to predict the scattering behavior such as ray-tracing and Monte Carlo techniques. Another approach would be to use a flexible negative mask that would be generated by taking a digital picture of the illuminated pouch and then printing the negative of this image on a transparent slide. Examples of such images are shown underneath the intensity images in Fig. 4. This mask could then be secured over the transparent top of the pouch. This would have the effect of attenuating the higher intensity regions, while providing a clear transparent path for the low-intensity regions, resulting in a more uniform light distribution, although at the expense of a reduced maximum light output. Several fibers, rather than a single fiber, could also be used in the pouch to provide a more evenly distributed light source. The light source and fiber coupling could be integrated and optimized for maximum light delivery to the pouch. Last, it should be noted that although visible light is used in this study, both infrared and ultraviolet wavelengths can also be used with appropriate choice of light source, delivery fiber, and scattering medium. Short-pulse light sources (e.g., lasers) can be used to provide very high photon fluxes and resolve phenomena at short time scales, although the illumination light would now be monochromatic, unless a white-light continuum were used.[14] The device may also be useful for the natural sciences and engineering, where space is limited. Examples include noninvasive physiological measures such as neurogenic inflammation, subdural blood flow observations, and cardiac output in clinical settings.[15]

Acknowledgments

The authors gratefully acknowledge Dr. Jim Quinn for assistance with the SEM imaging and wish to thank Mr. D. Bar-Kochba for his assistance in fabricating the pouches. M. Frame gratefully acknowledges partial support from NIH Grant No. HL55492 and AHA Grant No. 0655908T for this work.

References

1. R. Richards-Kortum and E. Sevick-Muraca, "Quantitative optical spectroscopy for tissue diagnosis," *Annu. Rev. Phys. Chem.* **47**, 555–606 (1996).
2. J. Lademann, A. Patzelt, M. Darvin, H. Richter, C. Antoniou, W. Sterry, and S. Koch, "Application of optical noninvasive methods in skin physiology," *Laser Phys. Lett.* **5**(5), 335–346 (2008).
3. J. T. Wessels, A. C. Busse, J. Mahrt, C. Dullin, E. Grabbe, and G. A. Mueller, "*In vivo* imaging in experimental preclinical tumor research—a review," *Cytometry, Part A* **71A**(8), 542–549 (2007).
4. D. L. Taylor, E. S. Woo, and K. A. Giuliano, "Real-time molecular and cellular analysis: the new frontier of drug discovery," *Curr. Opin. Biotechnol.* **12**(1), 75–81 (2001).
5. W. M. Ahmed, S. J. Leavesley, B. Rajwa, M. N. Ayyaz, A. Ghafoor, and J. P. Robinson, "State of the art in information extraction and quantitative analysis for multimodality biomolecular imaging," *Proc. IEEE* **96**(3), 512–531 (2008).
6. D. M. Owen, M. A. A. Neil, P. M. W. French, and A. I. Magee, "Optical techniques for imaging membrane lipid microdomains in living cells," *Semin Cell Dev. Biol.* **18**(5) 591–598 (2007).
7. K. W. Eliceiri and C. Rueden, "Tools for visualizing multidimensional images from living specimens," *Photochem. Photobiol.* **81**(5) 1116–1122 (2005).
8. W. Q. Ge and P. S. Khalsa, "Encoding of compressive stress during indentation by group III and IV muscle-mechano-nociceptors in rat *gracilis* muscle," *J. Neurophysiol.* **89**(2), 785–792 (2003).
9. G. Brattberg, M. G. Parker, and M. Thorslund, "A longitudinal study of pain: reported pain from middle age to old age," *Clin. J. Pain* **13**(2) 144–149 (1997).
10. M. F. Modest, *Radiative Heat Transfer*, McGraw-Hill, New York (1993).
11. R. J. Fox and M. D. Frame, "Regulation of flow and wall shear stress in arteriolar networks of the hamster cheek pouch," *J. Appl. Physiol.* **92**(20) 2080–2088 (2002).
12. C. F. Borhen and D. R. Huffman, *Absorption and Scattering of Light by Small Particles*, Wiley, New York (1983).
13. T. Wriedt, "A review of elastic light scattering theories," *Part. Part. Syst. Charact.* **15**(2) 67–74 (1998).
14. R. L. Fork, C. V. Shank, C. Hirlimann, R. Yen, and W. J. Tomlinson, "Femtosecond white-light continuum pulses," *Opt. Lett.* **8**(1) 1–3 (1983).
15. R. J. Rivers, J. B. Beckman, and M. D. S. Frame, "Technique for using video microscopy and indicator dilution for repeated measurements of cardiac output in small animals," *Anesthesiology* **94**(3) 489–495 (2001).